UNIVERSIDADE ESTADUAL DE CAMPINAS
SISTEMA DE BIBLIOTECAS DA UNICAMP
REPOSITÓRIO DA PRODUÇÃO CIENTIFICA E INTELECTUAL DA UNICAMP

Versão do arquivo anexado / Version of attached file:

Versão do Editor / Published Version

Mais informações no site da editora / Further information on publisher's website:
https://www.spiedigitallibrary.org/journals/optical-engineering/volume-57/issue-11/116107/Polymer-optical-fiber-specklegram-strain-sensor-with-extended-dynamic-range/10.1117/1.OE.57.11.116107.full

DOI: 10.1117/1.OE.57.11.116107

Direitos autorais / Publisher's copyright statement:
©2018 by SPIE - International Society for Optical Engineering . All rights reserved.

DIRETORIA DE TRATAMENTO DA INFORMAÇÃO

Cidade Universitária Zeferino Vaz Barão Geraldo
CEP 13083-970 – Campinas SP
Fone: (19) 3521-6493
http://www.repositorio.unicamp.br

Optical Engineering 57(11), 116107 (November 2018)

Polymer optical fiber specklegram strain sensor with extended dynamic range

Eric Fujiwara,[a,*] Luiz Evaristo da Silva,[b] Thiago H. R. Marques,[b] and Cristiano M. B. Cordeiro[b]
[a]University of Campinas, School of Mechanical Engineering, Laboratory of Photonic Materials and Devices, Campinas, Brazil
[b]University of Campinas, "Gleb Wataghin" Institute of Physics, Specialty Optical Fibers and Photonic Materials Laboratory, Campinas, Brazil

Abstract. A polymer optical fiber strain sensor with extended dynamic range is reported. The proposed algorithm resets the reference fiber status depending on the magnitude of the specklegram deviation so the correlation coefficient never saturates, yielding a continuous response over the full range for both positive and negative strains. The technique was evaluated on the measurement of axial strains using a ZEONEX core, poly(methyl methacrylate) cladding multimode fiber, presenting reproducible results with 3×10^{-3} $\mu\varepsilon^{-1}$ sensitivity (~15 $\mu\varepsilon$ resolution) within a 22,600 $\mu\varepsilon$ interval. In contrast to the available approaches, the presented method can retrieve the strain direction and does not require intensive image processing, thus providing a simple and reliable technique for mechanical measurements using multimode optical fibers. © *2018 Society of Photo-Optical Instrumentation Engineers (SPIE)* [DOI: 10.1117/1.OE.57.11.116107]

Keywords: fiber specklegram sensor; polymer optical fiber; optical fiber sensor; strain measurement.

Paper 181238 received Aug. 28, 2018; accepted for publication Nov. 14, 2018; published online Nov. 29, 2018.

1 Introduction

The measurement of strain and stress is essential in several technological fields, including structural health monitoring in civil construction[1] and aerospace[2] industries, biomedicine,[3] and robotics.[4] Even though the assessment of such microscale mechanical displacements can be accomplished by different types of invasive and noninvasive techniques,[5] optical fiber sensors have been extensively applied on practical strain measurements, especially due to their lightweight, high sensitivity, electrical insulation, remote and distributed sensing capabilities, and immunity to electromagnetic interference.[6]

Currently, several designs of optical fiber strain sensors have been proposed, such as fiber Bragg gratings[7] and long-period gratings,[8] in-fiber interferometers based on heterocore structures,[9] fiber tapers,[10] multimode interference fiber devices,[11] photonic crystal fibers,[12] and stimulated Brillouin scattering distributed sensors.[13] Although the aforementioned setups present notable performance in terms of sensitivity and resolution, most of these sensors rely on the realization of additional processes on the optical fibers—like grating fabrication and tapering—as well as on the utilization of precise and expensive interrogation systems.

In this context, fiber specklegram sensors (FSS) figure as promising alternatives to the usual sensing schemes since they can be implemented with multimode fibers (MMF) and conventional low-cost cameras, present high sensitivity (comparable to interferometric techniques) and can perform quasi-distributed measurements.[14–16] Indeed, successful applications of FSS have been reported concerning the assessment of displacement,[14] force,[17] temperature,[18] and chemical concentration.[19]

Recently, the use of polymer optical fibers (POF) has been investigated in order to increase the response of FSS. In addition to their intrinsic advantages over silica fibers, such as enhanced mechanical properties and ease of fabrication,[20] POF can also be designed with larger core dimensions, thus supporting a greater number of modes, which reflects on the improvement of the speckle field spatiotemporal characteristics.[15]

The interrogation of FSS is typically carried out by evaluating the correlation coefficient between the speckle field images obtained for a reference and an interrogated fiber status, making it possible to detect the subtle changes induced by the measured variable. In spite of the high sensitivity provided by such methodology, the dynamic range is limited by the saturation of the correlation coefficient,[14] which restricts its application to small strain values. Alternatively, the mechanical stimuli can be assessed by computing the differential correlation between the specklegrams acquired in consecutive frames,[21] so the response is never saturated for normal operating conditions. Although this method can be employed on displacement and vibration sensing, it is not possible to determine the stress direction and absolute value, once the reference frame is changed every iteration. Another approach is composed of performing a morphological processing over the acquired field images in order to identify the most representative light speckles (in terms of intensity and stability), so the correlation is evaluated for tracking their spatiotemporal variations.[22] This technique can be utilized for performing strain measurements with high sensitivity and improved dynamic range, but additional steps of image processing and features extraction are required, which increases the computational complexity.

In this sense, the present paper reports a POF strain sensor based on fiber specklegram analysis with automatic dynamic range extension. The reference fiber status is reset depending on the magnitude of the speckle field deviation, so the correlation coefficient never saturates. Moreover, in contrast to the differential approach, it is possible to detect the strain

*Address all correspondence to Eric Fujiwara, E-mail: fujiwara@fem.unicamp.br

0091-3286/2018/$25.00 © 2018 SPIE

Downloaded From: https://www.spiedigitallibrary.org/journals/Optical-Engineering on 08 Oct 2019
Terms of Use: https://www.spiedigitallibrary.org/terms-of-use

direction by using an additional reference specklegram, yielding a continuous response over the full range with sensitive and reproducible results.

2 Fundamental

2.1 *Optical Fiber Specklegram*

When the light from a coherent source is guided through a MMF, a speckle-like pattern emerges at the fiber end face. This specklegram is produced due to the interference between the several propagating modes and its characteristics change with the waveguide conditions, causing the modal noise.[23] Even though such phenomenon must be avoided in optical communication systems, actually the speckle fields contain precise and reproducible information about the fiber status,[14,24] making it suitable for sensing applications.

Given the complex amplitude $A(x,y)$ of the M guided modes:

$$A(x,y)=\sum_{m=0}^{M-1} a_m(x,y)\exp[j\varphi_m(x,y)], \tag{1}$$

where $a_m(x,y)$ and $\phi_m(x,y)$ are the amplitude and phase distributions, respectively, of the m'th mode. The intensity $I(x,y)$ of a specklegram projected over an xy plane is denoted by Ref. 14:

$$I(x,y)=\sum_{m=0}^{M-1}\sum_{n=0}^{M-1} a_m a_n \exp[j(\varphi_m-\varphi_n)], \tag{2}$$

therefore, the intensity distribution varies according to the modal phasing deviations caused by the external stimuli.

The number of visible speckles is approximately equal to the number of guided modes M. Assuming that the modal power distribution is uniform within the core region, the M value for a step-index fiber can be calculated by

$$M=\frac{V^2}{2}=\frac{(rk_0\mathrm{NA})^2}{2}, \tag{3}$$

where V is the normalized frequency, r is the core radius, k_0 is the light free-space propagation constant, and NA is the fiber numerical aperture.[25] As previously mentioned, larger core POF can be used for increasing M and, consequently, the number of features in the specklegram images, thus improving the fiber sensitivity to the external stimuli.[26] In practice, the M value is much lower than the estimated by Eq. (3) since the optical setup is based on a Gaussian beam launching, so the light is preferably coupled to the LP_{0m} modes.[27] On the other hand, subtle misalignments caused by lens defocusing, as well as angular and axial offsets cause the modal power to the distributed to the high-order modes, so the characteristics of the projected speckle field strongly depend on the launching conditions.[28]

2.2 *Specklegram Correlation with Dynamic Range Extension*

Consider the specklegrams $I(x,y)$ measured for the interrogated fiber status and $I_0(x,y)$ obtained for a reference condition. The subtle differences between I and I_0 induced by the external variable can be quantified with the evaluation of the zero-mean normalized cross-correlation (ZNCC):

$$\mathrm{ZNCC}=\frac{\int\int(I_0-\bar{I}_0)(I-\bar{I})\mathrm{d}x\mathrm{d}y}{[\int\int(I_0-\bar{I}_0)^2\mathrm{d}x\mathrm{d}y\int\int(I-\bar{I})^2\mathrm{d}x\mathrm{d}y]^{1/2}}, \tag{4}$$

where $\bar{I}_0$ and $\bar{I}$ are the average intensity values for the reference and the current fiber statuses, respectively.[29] In comparison to the simple normalized correlation coefficient,[14] the ZNCC suppresses variations in the image brightness, providing a more robust response.[29]

As observed in Eq. (4), ZNCC $=1$ when I matches I_0, whereas its value is decreased as the current specklegram deviates from the reference one, until it reaches a saturation level from which the differences between I and I_0 become too large. A possible approach for extending the measurement interval is composed of periodically resetting the reference speckle field image,[14] so the ZNCC is restored to 1 and the FSS sensitive region is shifted. Additionally, since the specklegram characteristics are reversible under controlled conditions, one may attempt to evaluate the correlation coefficients referenced to several calibration points, making it possible to characterize the fiber statuses over the full measurement range, but, in practice, performing such intensive calibration may be laborious and demand considerable computer processing.

The methodology proposed in this work for extending the dynamic range is based on calculating the ZNCC for two reference statuses $I_{0\mathrm{A}}$ and $I_{0\mathrm{B}}$, yielding $\mathrm{ZNCC_A}$ and $\mathrm{ZNCC_B}$, respectively. The $\mathrm{ZNCC_B}$ is compared to a threshold value τ_B for each iteration, so given the current specklegram I, if $\mathrm{ZNCC_B}\leq\tau_\mathrm{B}$, the reference is set to $I_{0\mathrm{B}}=I$, causing $\mathrm{ZNCC_B}$ to be restored to 1. This situation occurs when the fiber disturbance increases in modulus in one direction, for example, a tensile axial stress. In order to keep the previous reference, the $\mathrm{ZNCC_A}$ is set to $I_{0\mathrm{A}}=I_{0\mathrm{B}}$ before updating $I_{0\mathrm{B}}$.

Conversely, if the external stimulus is applied in the opposite direction, such as a compressive load, the $\mathrm{ZNCC_B}$ will tend to increase as the current specklegram gets correlated with the reference status, reaching $\mathrm{ZNCC_B}=1$ when $I=I_{0\mathrm{B}}$ because the speckle field changes are reversible. However, the $\mathrm{ZNCC_B}$ value will start to decrease again as the negative strain is increased because I will depart from the reference point $I_{0\mathrm{B}}$, so it is not possible to retrieve the strain direction due to the ambiguity of the ZNCC curve behavior. On the other hand, once $I_{0\mathrm{A}}$ retains the previous calibration, the $\mathrm{ZNCC_A}$ will increase monotonically even if the $\mathrm{ZNCC_B}$ reaches its turning point for the fiber statuses comprised between $I_{0\mathrm{A}}$ and I. In this sense, $\mathrm{ZNCC_A}$ can be compared to another threshold value τ_A, and consequently, the strain direction is reversed if $\mathrm{ZNCC_A}\geq\tau_\mathrm{A}$.

The extended zero-mean normalized cross-correlation (EZNCC) coefficient is therefore evaluated as follows:

$$\mathrm{EZNCC}=\mathrm{EZNCC}_0\mp(\mathrm{ZNCC_B}-1), \tag{5}$$

where EZNCC_0 is a cumulative offset due to the ZNCC curve reset, and the term $(\mathrm{ZNCC_B}-1)$ can be negative or positive for tensile or compressive strains, respectively. The algorithm for automatic EZNCC evaluation is shown in Table 1.

Downloaded From: https://www.spiedigitallibrary.org/journals/Optical-Engineering on 08 Oct 2019
Terms of Use: https://www.spiedigitallibrary.org/terms-of-use

Table 1 Algorithm for EZNCC evaluation.

Function EZNCC

Input: I, I_{0A}, I_{0B}, $EZNCC_0$, sign

Output: EZNCC

$ZNCC_A \leftarrow ZNCC(I, I_{0A})$

$ZNCC_B \leftarrow ZNCC(I, I_{0B})$

if $ZNCC_B \leq \tau_B$

$I_{0A} \leftarrow I_{0B}$

$I_{0B} \leftarrow I$

$EZNCC_0 \leftarrow EZNCC$

elseif $ZNCC_A \geq \tau_A$ and sign $= -1$

sign $\leftarrow -$ sign

$EZNCC \leftarrow EZNCC_0 + \text{sign} * (ZNCCB - 1)$

return EZNCC

3 Materials and Methods

3.1 *Fabrication of Polymer Optical Fiber*

The POF used on this work was fabricated at the Specialty Optical Fibers Laboratory, UNICAMP,[30] and is formed by two materials, a poly(methyl methacrylate) (PMMA) cladding and a cyclo-olefin polymer (ZEONEX 480R®)[31] central core.

First, ZEONEX pellets were extruded to a 1.3-mm thick filament in a vertical extruder. Such thread was inserted in a 70-mm PMMA rod with a central hole to form the fiber preform. Next, the preform was taken to a polymer pulling tower and pulled into a 12-mm cane. This intermediate process is carried out in order to avoid major structural deformations in the fiber.

The last fabrication step included drawing the cane to a fiber stage. The procedure was conducted with the real-time control of the process parameters, such as the furnace temperature (~215°C), preform feed speed (typically ~1 mm/min), fiber pulling speed (typically around few m/min), and fiber tension, whereas the fiber external diameter was constantly monitored by a laser meter. Negative pressure was applied to the cane to minimize air gaps in the core/cladding interface. Fiber tension was kept at low values (<100 g) during the drawing in order to produce a fiber that can be easily cleaved with a sharp razor blade.[32]

The photograph of the fabricated POF is shown in Fig. 1. The waveguide presents step-index profile (core and cladding refractive indexes of 1.52 and 1.49 in the visible wavelength, respectively), with cladding and core diameters of 450 and 70 μm, respectively.

3.2 *Experimental Setup*

The measurement setup is depicted in Fig. 2. The light emitted by a He–Ne laser source (Newport, continuous-wave, 633 nm) is launched into the ~40-cm length polymer fiber by means of an optical alignment system and an objective lens (20× magnification, NA = 0.40). The waveguide was carefully manipulated and cleaved at room temperature by using a razor blade, followed by verification of the fiber end face conditions using a microscope, as the end face conditions can modify the angular distribution of the output light. Next, the waveguide is slightly stretched and fixed to a mechanical stage, and then the output specklegram is projected over a plane surface by using an objective lens (NA = 0.40). Finally, the ~10 cm diameter speckle field image is recorded using a CCD camera (uEye IDS UI-2230SE-C-HQ, 1/3" size color sensor, 1024 × 768 pixels resolution, 15 fps rate) and processed by routines programmed in MATLAB, Mathworks.

Regarding the fiber launching, it is worth noticing that the setup was adjusted so the light was mostly confined inside the core region. Such procedure is important to reduce the contribution of the cladding modes, once the extraneous refractive index changes induced at the PMMA–air interface can result in specklegram fluctuations due to the possible coupling between core and cladding modes,[33] and thus compromise the repeatability of the measurements.

The experiments were conducted at room temperature and in the absence of mechanical vibrations, which could affect the specklegram formation and stability. Moreover, the measurements were carried out in a dark environment in order to minimize the influence of external illumination during the images acquisition.

For the assessment of strain sensitivity, a ~8.4 cm section of the fiber is attached to a linear stage, being one extremity connected to the moving part, whereas the other side is

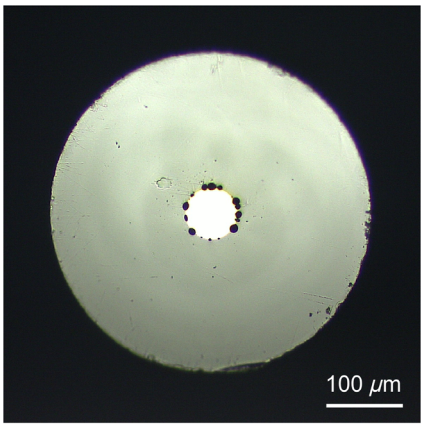

Fig. 1 Cross-section view of the POF end face.

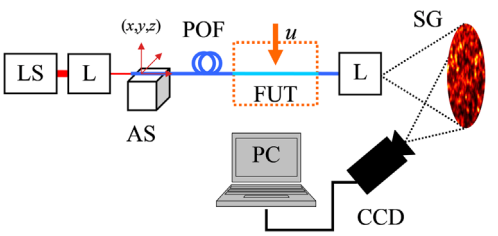

Fig. 2 Experimental setup. LS: laser source; L: objective lens; AS: fiber alignment stage; POF: polymer fiber; SG: specklegram projected over flat surface; CCD: camera. The fiber section under test (FUT) is excited by the controlled external stimulus u.

Downloaded From: https://www.spiedigitallibrary.org/journals/Optical-Engineering on 08 Oct 2019
Terms of Use: https://www.spiedigitallibrary.org/terms-of-use

firmly fixed to a static support to prevent slip. The system is controlled by a linear stepper motor (Newport ESP301, 0.001 mm/step), making it possible to apply precise axial loads.

3.3 *Data Analysis*

The data analysis procedure is presented in Fig. 3. Given the projected speckle field, a square 51×51 pixels region-of-interest (RoI) is defined at the specklegram center for comprising most of the visible light peaks and eliminating the border effects. Next, the acquired image in RGB space is converted to grayscale and then filtered by 2-D discrete wavelet transform (Daubechies db4) for denoising. Finally, the processed images are submitted to the ZNCC calculation frame-by-frame, so the obtained values can be correlated to the measured variables by frames synchronization. It is worth noticing that the RoI size was determined after preliminary tests: even though larger images can improve the sensitivity because of the amount of pixels to be compared during the ZNCC evaluation,[26] there are some drawbacks concerning the ZNCC algorithm processing time especially regarding the application of the wavelet filter, so the 51×51 pixels RoI provided the more reliable results concerning both scenarios.

4 Results and Discussion

4.1 *Analysis of Specklegrams Stability*

Even though the launching setup was adjusted to confine the light inside the core region, a part of the incident beam is still expected to be coupled to the cladding modes. Typical schemes for FSS interrogation perform the specklegram image acquisition by means of a camera or a detector array directly placed in front of the fiber end face,[14,15,21,34] but the cladding modes should be stripped in order to make the measurements more robust to the environmental effects. In particular, the fabricated POF was not coated with an external jacket since it could change the fiber mechanical properties and reduce the sensitivity to the applied strains, so the contribution of the cladding modes is not removed by a higher refractive index buffer, making it difficult to conduct the direct specklegram analysis in the near-field.

Alternatively, the light speckles bounded to the fiber core can be separated from the cladding ones by projecting the output specklegram over a flat surface instead of the camera plane, so the cross-correlation is evaluated by considering only the core propagating modes and the measurements can be conducted without covering the fiber with index matching liquids. To demonstrate such improvements on the specklegram stability, the POF was initially kept in the absence of external stimuli, whereas the projected speckle field was recorded for 500 frames. After that, the experiment was repeated by maintaining the same launching setup, but the objective lens was removed and the camera was placed in front of the fiber end face in order to capture the output light.

As observed in Fig. 4, the ZNCC evaluated for the projected speckle field presents a slight decay and then stabilizes at ZNCC $\cong 0.95$. The correlation coefficient is not locked to 1 probably due to variations on environmental conditions, but such offset does not affect the sensor response in a significant manner. It is also worth noticing that the target plane was kept stationary during the tests, so the effects related to the surface texture and motion can be neglected.

On the other hand, the ZNCC obtained from the directly acquired specklegram (Fig. 4) exhibited a drastic decrease after ~50 frames (3.3 s), reaching the stabilization for ZNCC $\cong 0.77$. Given that the camera was placed at a relatively short distance (~50 mm) from the fiber end face, the acquired images contain superposed information from both core and cladding propagating modes. As the latter is more susceptible to the external effects at the cladding–air interface, especially the high-order modes,[35] a granular pattern that undergoes dynamically spatiotemporal changes is produced, yielding fluctuations in the pixels values and thus inducing the correlation loss.

The stabilization of the ZNCC value can be explained as follows. As previously mentioned, the correlation coefficient decreases as the current specklegram I deviates from the reference one I_0. Since the fiber was maintained under the undisturbed status during the experiments, the variations in the pixel values were solely caused by the moving grains (modulated by the cladding modes), and not by light attenuation or mode coupling due to fiber bending, for example.

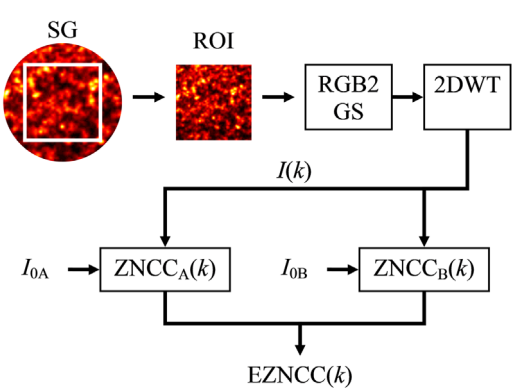

Fig. 3 Diagram of specklegram analysis: a RoI is extracted from the projected specklegram (SG), resulting in an RGB image, which is converted to grayscale (GS) and then filtered by 2-D discrete wavelet transform (2DWT). Finally, the intensity of the k'th frame $I(k)$ is correlated to the references I_{0A} and I_{0B} in order to obtain the $ZNCC_A$ and $ZNCC_B$ for each frame, and consequently, the extended correlation coefficient EZNCC(k).

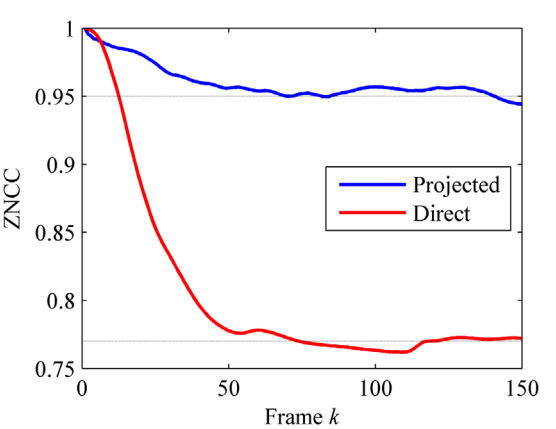

Fig. 4 Variation of ZNCC for an undisturbed POF regarding the analysis of the projected and the directly measured specklegrams.

Downloaded From: https://www.spiedigitallibrary.org/journals/Optical-Engineering on 08 Oct 2019
Terms of Use: https://www.spiedigitallibrary.org/terms-of-use

Consequently, the intensity of particular pixels will tend to depart or to be restored to the reference condition depending on the fluctuation of light speckles, so even though I continues changing, some pixels will get correlated again and the overall contribution of the pixels prevents the ZNCC to keep decreasing with time.

In order to elucidate such phenomenon, the specklegram images for the k'th frame $I(k)$ were compared to the initial fiber status $I_0 = I(1)$, so the variations between the speckle fields can be evaluated in terms of the absolute difference $\Delta I = |I(k) - I_0|$. In this sense, as the ΔI overall value increases, the correlation between $I(k)$ and I_0 is lost, causing the NIPC do decrease. The results of the projected specklegram analysis are illustrated in Fig. 5(a) regarding the frames $k = 1$, 10, 25, and 50. Even though the principal light peaks are preserved in terms of amplitude and position, the eventual fluctuations in the experimental setup induce slight variations in the pixel values, affecting the correlation coefficient so the ZNCC was not maintained at 1.

Conversely, the direct acquisition, Fig. 5(b), yields small grains that behave like a noise in the output image, increasing the absolute difference with time and making it difficult to obtain reproducible measurements. It is worth noticing that part of the light speckles was still preserved in this case, being related to the core propagating modes, making it possible to perform practical sensing by utilizing the morphological operations technique.[22] Moreover, one can attempt to apply digital filters[36] or statistical analysis[23] for suppressing the noise, but important information regarding the fiber status can be lost during such data reduction step.

4.2 *Strain Measurements*

The sensor response to axial strain was evaluated by adjusting the controller to move from 0 to 0.03 mm in steps of 0.003 mm and keeping each load value during 100 acquisition frames, and then computing the ZNCC with respect to the undisturbed status. The results regarding the average of three upscale/downscale experiments are shown in Fig. 6(a),

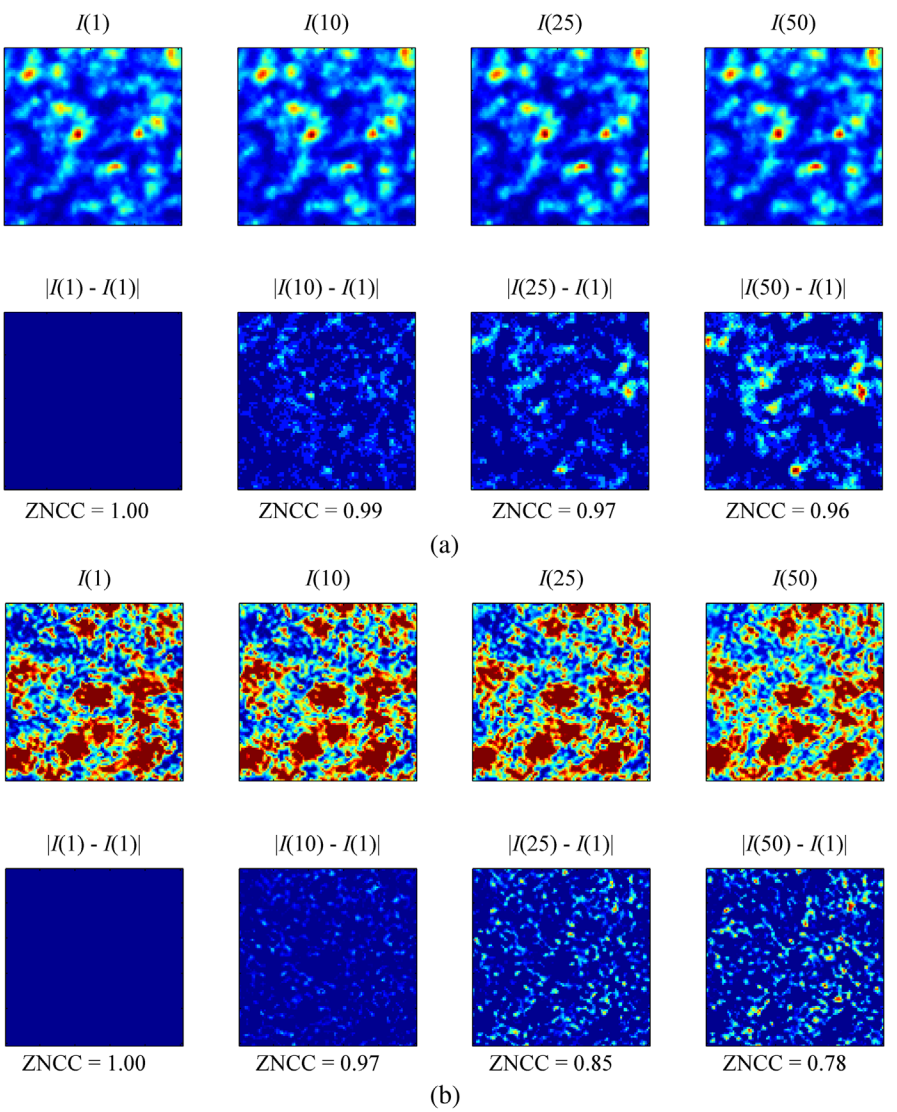

Fig. 5 Specklegram images $I(k)$ obtained by (a) projection and (b) direct acquisition methods. The bottom images show the absolute difference between the specklegrams for the k'th and the reference (first) frames. The ZNCC(k) values are also displayed for each frame. The intensity values were normalized for the sake of visualization.

Downloaded From: https://www.spiedigitallibrary.org/journals/Optical-Engineering on 08 Oct 2019
Terms of Use: https://www.spiedigitallibrary.org/terms-of-use

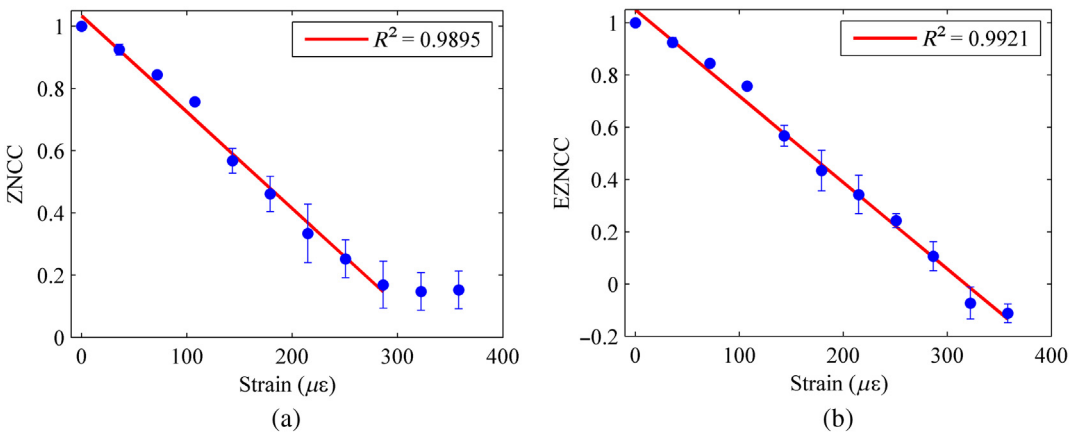

Fig. 6 Sensor static response: (a) ZNCC and (b) EZNCC as a function of axial strain. The solid line indicates the linear curve fitting.

with the linear displacements converted to microstrains ($\mu\varepsilon$). Since the specklegram aspect undergoes spatial changes as the strain magnitude is increased, the ZNCC tends to decrease until it saturates at ~0.15. Since the sensor presents a linear response within the 0 to 285 $\mu\varepsilon$ range, one may obtain the static response from the angular coefficient of the curve fitting, yielding 3.10×10^{-3} $\mu\varepsilon^{-1}$ sensitivity. Assuming a detectable variation of $\Delta\text{ZNCC} = 0.05$, the strain resolution can be estimated as $0.05/3.10 \times 10^{-3} \cong 16.13$ $\mu\varepsilon$.

Next, the EZNCC was computed for the same previous data, yielding the calibration curve presented in Fig. 6(b). For convenience, the thresholds were set to $\tau_A = \tau_B = 0.5$, which means that the correlation coefficient is reset when $\text{ZNCC}_B \leq 0.5$, but these values can be adjusted to any setpoint over the saturation limit of the ZNCC. In this case, the dynamic range was extended to the full range (358 $\mu\varepsilon$) resulting in a 3.31×10^{-3} $\mu\varepsilon^{-1}$ sensitivity and $0.05/3.31 \times 10^{-3} \cong 15.11$ $\mu\varepsilon$ estimated strain resolution, indicating that the measurement interval was successfully improved without compromising the sensor gain.

In order to demonstrate the repeatability of the measurements, the POF was subjected to cyclic strains within the linear range, in which the moving stage was programmed to translate from 0 to 0.024 mm with 0.003 mm steps by keeping the static load for 50 frames and then return to the initial position. This procedure was repeated six times, yielding input strain values ranging from 0 to ~286 $\mu\varepsilon$, and the hysteresis uncertainty u_h was obtained by calculating the average of the absolute difference between upscale and downscale data divided by the full scale for each period.

The sensor response in terms of ZNCC for two periods is shown in Fig. 7(a), demonstrating that the correlation coefficient value is practically recovered at the end of the loading cycle. Since the speckle field changes were reversible, the waveguide structure was probably not modified during the experiments, so the measurements were repeatable within the tested interval. The summarized results for six repetitions yielded low hysteresis with $u_h = 3.34\%$.

Regarding the EZNCC, the extended cross-correlation was evaluated for $\tau_A = \tau_B = 0.5$, providing the results illustrated in Fig. 7(b). It is observed that the sensor response was more linear than the obtained for the ZNCC because the reference is reset before the correlation curve approaches to the saturation value, whereas in Fig. 7(a), the sensitivity is decreased if the axial loading is close to the maximum strain. Moreover, in contrast to the available techniques,[14,21] the proposed method allows for preserving the stress direction in addition to the dynamic range extension since the sensor characteristics are still reversible. The hysteresis uncertainty calculated for the EZNCC was $u_h = 3.73\%$, which is comparable to the ZNCC.

Finally, to demonstrate the sensor operation for a larger strain interval, the POF was subjected to 1.9 mm total deformation (corresponding to ~22600 $\mu\varepsilon = 22.6$ mε) by moving the stage with steps of 0.01 mm. A comparison of the results obtained for the ZNCC and EZNCC for the 1-mε interval is depicted in Fig. 8. Due to the magnitude of the strain increments, the ZNCC rapidly saturates after ~0.3 mε, but the EZNCC response remains linear as the reference specklegram is conveniently updated (both threshold values were set to 0.5). Concerning the analysis for the full range, one may observe in Fig. 9(a) that the sensor static characteristics were notably improved in relation to the conventional cross-correlation analyses, providing a linear response with 3.02 mε^{-1} (3.02×10^{-3} $\mu\varepsilon^{-1}$) sensitivity. At last, a compressive stress was simulated by reversing the specklegram change history in order to show the ability of the proposed technique to detect the strain direction even in the case of larger deformations. As shown in Fig. 9(b), the tensile and compressive stimuli can be properly distinguished without requiring the assignment of absolute reference points, making the ENZCC more versatile than the differential correlation analysis.

In addition to the stability of the sensor static characteristics, it is worth noticing that the POF supported a relatively high deformation value (above the elastic limit) without suffering rupture, which exceeds the practical limits of silica fiber sensors. Moreover, even though optical losses were expected for a mechanically loaded condition,[37] the FSS sensitivity was not significantly degraded for extreme strain values, so the contribution of the changes on light speckles configuration will impact more on the correlation calculus than the average light intensity.

The sensor sensitivity can be still enhanced by making some improvements in the experimental setup. Examples include choosing the appropriate objective lens NA,[28]

Downloaded From: https://www.spiedigitallibrary.org/journals/Optical-Engineering on 08 Oct 2019
Terms of Use: https://www.spiedigitallibrary.org/terms-of-use

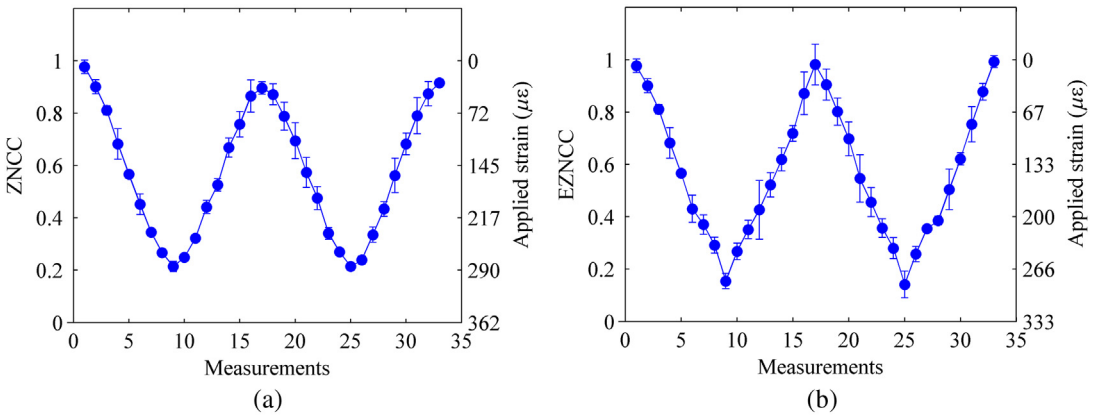

Fig. 7 Sensor response to a periodical strain cycle: (a) ZNCC and (b) EZNCC. The axis in the right side indicates the input strain values.

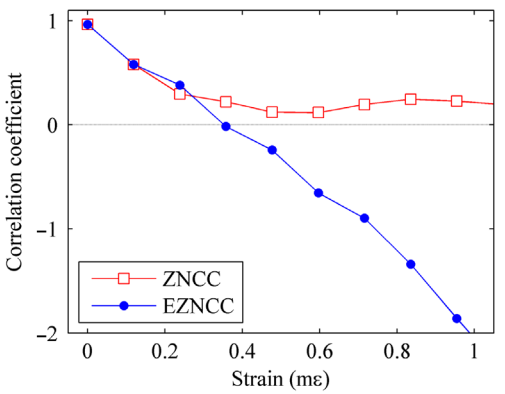

Fig. 8 Comparison of ZNCC and EZNCC for the 1-mε strain range. The solid lines are guides for the eye.

applying a controlled axial offset in the launching setup,[38] and using mode scramblers based on macro- and microcurvatures. These techniques allow for controlling the power distribution, so it is possible to excite a higher number of modes or select the more appropriate ones,[39] making the specklegram spatiotemporal changes more evident.

In spite of the reported results, some considerations must be taken in account concerning the application of the proposed sensor in practical measurements. As observed in all types of FSS, the output speckle field is very sensitive to any change in the light guiding condition induced by the fiber refractive index modulation. Remarkably, mechanical disturbances, such as vibration and bending, can produce correlation losses due to changes in the specklegram configuration and lead to inaccurate strain values. The first case can be compensated by statistical methods or frequency domain analyses since the speckle field modulation caused by moderate is reversible, whereas its average intensity remains constant,[34] but the latter generates systematic errors that are complicated to be amended by using optical techniques.[40] Therefore, except by the sensing region, the fiber should be enclosed in a rigid structure for avoiding the extraneous mechanical effects.

Another aspect is the temperature sensitivity of the POF. Although the detection scheme was optimized for neglecting the contribution of the cladding modes, thermal oscillations can affect the refractive index and the structural properties of the cladding material, yielding changes in the guiding conditions within the core region. The specklegram is also sensitive to source wavelength shifts, as the modal phase

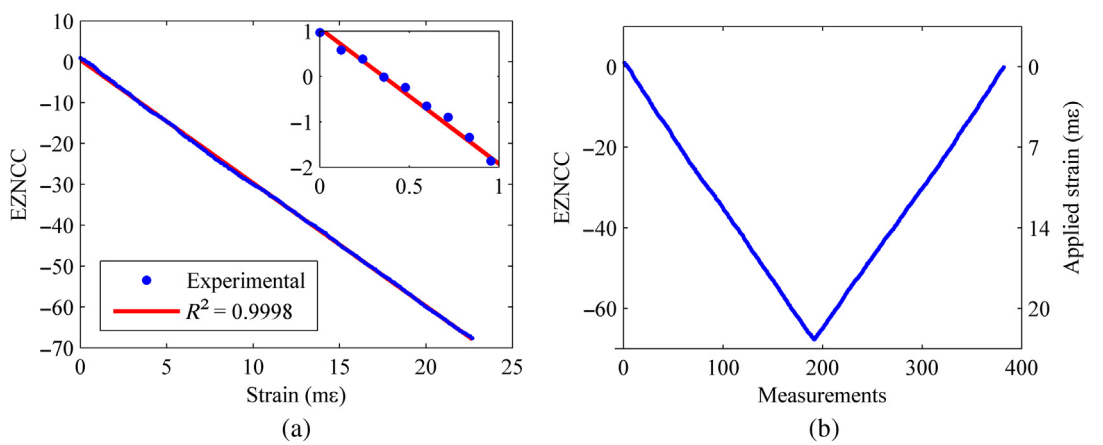

Fig. 9 Strain measurements with extended dynamic range: (a) variation of EZNCC as a function of the strain for a 22.6 mε range, with experimental data fitted by linear function. The inset details the EZNCC for the 1 mε range and (b) variation of EZNCC as a function of the applied strain for a tensile-compressive load.

Downloaded From: https://www.spiedigitallibrary.org/journals/Optical-Engineering on 08 Oct 2019
Terms of Use: https://www.spiedigitallibrary.org/terms-of-use

deviation is modulated by the wavelength-dependent mode propagation constant,[41,42] causing the output speckle field to undergo spatiotemporal changes even though the fiber is kept at an undisturbed condition. Finally, the specklegram tends to drift for long period measurements due to fluctuations in the laser source power or in the launching setup alignment, resulting in systematic changes in the reference fiber status and yielding calibration loss. It is worth noticing that the EZNCC per se is not capable of properly resolving the fiber strain if the speckle field experiences such extraneous effects since the correlation loss will be recognized as an intentional change in the waveguide status and then interpreted as a gradually applied load.

In this context, a straightforward approach for temperature, wavelength shift, and drift compensation consists of using an additional reference fiber subjected to the same operation environment, but not bounded to the strain source, similarly to the practiced in some FBG-based schemes.[1] Considering both reference and measurement fibers connected to the same launching waveguide by means of a coupler, the drift-induced changes are expected to be visualized in both projected specklegrams with the same temporal characteristics. In this case, the specklegram changes caused by extraneous effects will be probably superposed to the strain information in the correlation curve, thus, one can isolate the mechanical effect by dividing the probe by the reference signal, or by resetting I_0 if the ZNCC for the reference fiber is reduced below a threshold value. It is worth noticing that the sensor response is not saturated because of the EZNCC algorithm, so the system can perform over a wide range of temperature fluctuation. Nevertheless, it is possible to choose the proper materials for the POF fabrication in order to make the fiber more robust to thermal effects.[43]

5 Conclusion

The methodology for extending the FSS dynamic range was successfully implemented on the interrogation of a POF strain sensor. The system provided a $\sim 3 \times 10^{-3}$ $\mu\varepsilon^{-1}$ sensitivity (~ 15 $\mu\varepsilon$ resolution) within the 22,600 $\mu\varepsilon$ measurement interval, and in contrast to the available techniques, the proposed approach can retrieve the magnitude and direction of the applied load without requiring intensive calibration or complicated image processing algorithms. Moreover, it is possible to improve the robustness of the FSS by acquiring the specklegram projected from the core region, so the influence of cladding propagating modes can be neglected.

Even though additional developments in terms of POF design and speckle field processing are still necessary in order to achieve the resolution obtained for currently available FBG systems (typically, a 1 pm wavelength resolution can resolve variations from 0.5 to 1 $\mu\varepsilon$[44]), it must be stressed that the specklegram-based approach can be implemented with a much simpler and inexpensive interrogation setup. Finally, even though the methodology was demonstrated to strain measurements, it is important to notice that the speckle field projection analysis can be also applied to other types of FSS, such as on the assessment of temperature, current, and chemical concentration.

Disclosures

The authors declare that there are no conflicts of interests regarding the publication of this article.

Acknowledgments

This work was supported by the Sao Paulo Research Foundation (FAPESP) [Grant Nos: 2017/25666-2 and 2014/50632-6]; the Conselho Nacional de Desenvolvimento Científico e Tecnológico (CNPq); and the Coordenação de Aperfeiçoamento de Pessoal e Nível Superior (CAPES).

References

1. M. Majumder et al., "Fiber Bragg gratings in structural health monitoring—present status and applications," *Sens. Actuators A: Phys.* **147**(1), 150–164 (2008).
2. A. Panopoulou et al., "Dynamic fiber Bragg gratings based health monitoring system of composite aerospace structures," *Acta Astronaut.* **69**(7–8), 445–457 (2011).
3. V. Mishra et al., "Fiber grating sensors in medicine: current and emerging applications," *Sens. Actuators A: Phys.* **167**(2), 279–290 (2011).
4. A. Amjadi et al., "Stretchable, skin-mountable, and wearable strain sensors and their potential applications: a review," *Adv. Funct. Mater.* **26**(11), 1678–1698 (2016).
5. C. S. Lynch, "Strain measurement," in *Measurement, Instrumentation, and Sensors Handbook: Spatial, Mechanical, Thermal, and Radiation Measurement*, J. G. Webster and H. Eren, Eds., Vol. **37**, pp. 1–18, CRC Press, Boca Raton (2014).
6. B. Culshaw, "Optical fiber sensor technologies: opportunities and—perhaps—pitfalls," *J. Lightwave Technol.* **22**(1), 39–50 (2004).
7. B. Torres et al., "Analysis of the strain transfer in a new FBG sensor for structural health monitoring," *Eng. Struct.* **33**(2), 539–548 (2011).
8. Y. Huang et al., "A temperature self-compensated LPFG sensor for large strain measurements at high temperature," *IEEE Trans. Instrum. Meas.* **59**(11), 2997–3004 (2010).
9. Z. Xu et al., "Volume strain sensor based on spectra analysis of in-fiber modal interferometer," *IEEE Sens. J.* **13**(6), 2139–2145 (2013).
10. Z. Tian and S. S-H. Yam, "In-line abrupt taper optical fiber Mach-Zehnder interferometric strain sensor," *IEEE Photonics Technol. Lett.* **21**(3), 161–163 (2009).
11. R. M. André et al., "Strain-temperature discrimination using multimode interference in tapered fiber," *IEEE Photonics Technol. Lett.* **25**(2), 155–158 (2013).
12. L. M. Hu et al., "Photonic crystal fiber strain sensor based on modified Mach-Zehnder interferometer," *IEEE Photonics J.* **4**(1), 114–118 (2012).
13. Y. Mizuno et al., "Brillouin scattering in multi-core optical fibers for sensing applications," *Sci. Rep.* **5**, 11388 (2015).
14. F. T. S. Yu et al., "Submicrometer displacement sensing using inner-product multimode fiber speckle fields," *Appl. Opt.* **32**(25), 4685–4689 (1993).
15. L. Rodriguez-Cobo, M. Lomer, and J-M. Lopez-Higuera, "Fiber specklegram-multiplexed sensor," *J. Lightwave Technol.* **33**(12), 2591–2597 (2015).
16. E. Fujiwara, M. F. M. Santos, and C. K. Suzuki, "Measurement of multipoint displacements by optical fiber specklegram sensor," in *Proc. of IEEE on Microwave and Optoelectronics Conf. (IMOC)*, IEEE, pp. 1–5 (2017).
17. E. Fujiwara et al., "Development of a tactile sensor based on optical fiber specklegram analysis and sensor data fusion technique," *Sens. Actuators A: Phys.* **263**, 677–686 (2017).
18. T. Okamoto and I. Yamaguchi, "Multimode fiber-optic Mach-Zehnder interferometer and its use in temperature measurement," *Appl. Opt.* **27**(15), 3085–3087 (1988).
19. E. Fujiwara, Y. T. Wu, and C. K. Suzuki, "Vibration-based specklegram fiber sensor for measurement of properties of liquids," *Opt. Lasers Eng.* **50**(12), 1726–1730 (2012).
20. K. Peters, "Polymer optical fiber sensors—a review," *Smart Mater. Struct.* **20**(1), 013002 (2011).
21. F. M. Reis et al., "Structural health monitoring suitable for airborne components using the speckle pattern in plastic optical fibers," *IEEE Sens. J.* **17**(15), 4791–4796 (2017).
22. L. Rodriguez-Cobo et al., "Optical fiber strain sensor with extended dynamic range based on specklegrams," *Sens. Actuators A: Phys.* **203**, 341–345 (2013).
23. N. Takai and T. Asakura, "Statistical properties of laser speckles produced under illumination from a multimode optical fiber," *J. Opt. Soc. Am. A* **2**(8), 1282–1290 (1985).
24. M. Plöschner, T. Tyc, and T. Čižmár, "Seeing through chaos in multimode fiber," *Nat. Photonics* **9**(8), 529–535 (2015).
25. K. O. Hill, Y. Tremblay, and B. S. Kawasaki, "Modal noise in multimode fiber links: theory and experiment," *Opt. Lett.* **5**(6), 270–272 (1980).
26. E. Fujiwara, M. F. M. Santos, and C. K. Suzuki, "Optical fiber specklegram sensor analysis by speckle pattern division," *Appl. Opt.* **56**(6), 1585–1590 (2017).

Downloaded From: https://www.spiedigitallibrary.org/journals/Optical-Engineering on 08 Oct 2019
Terms of Use: https://www.spiedigitallibrary.org/terms-of-use

27. W. A. Gambling, D. N. Payne, and H. Matsumura, "Mode excitation in a multimode optical-fibre waveguide," *Electron. Lett.* **9**(18), 412–414 (1973).
28. T. Tsuji, T. Asakura, and H. Fujii, "Variation of the speckle contrast in a graded-index fibre by misalignment of the incident beam," *Opt. Quantum Electron.* **16**(1), 9–18 (1984).
29. L. Di Stefano, S. Mattoccia, and F. Tombari, "ZNCC-based template matching using bounded partial correlation," *Pattern Recognit. Lett.* **26**(14), 2129–2134 (2005).
30. C. M. B. Cordeiro, J. G. Hayashi, and T. H. R. Marques, "Microstructured polymer fibers in Brazil," in *22nd Int. Conf. Plastic Optical Fibers (POF 2013)*, pp. 295–297 (2013).
31. Zeon Corporation, "ZEONEX®–cyclo olefin polymer (COP)," 2016, www.zeon.co.jp/content/200181690.pdf
32. G. Barton et al., "Fabrication of microstructure polymer optical fibres," *Opt. Fiber Technol.* **10**(4), 325–335 (2004).
33. J. Tremblay, B. S. Kawasaki, and K. O. Hill, "Modal noise in optical fiber: open and closed speckle pattern regimes," *Appl. Opt.* **20**(9), 1652–1655 (1981).
34. W. B. Spillman et al., "Statistical-mode sensor for fiber optic vibration sensing uses," *Appl. Opt.* **28**(15), 3166–3176 (1989).
35. J. F. Huang, Y-J. Lee, and Y-L. Lo, "Spectrum analysis of high-order cladding modes based on long-period fiber gratings," *Opt. Eng.* **45**(9), 095001 (2006).
36. P. Etchepareborda, A. Federico, and G. H. Kaufmann, "Sensitivity evaluation of dynamic speckle activity measurements using clustering methods," *Appl. Opt.* **49**(19), 3753–3761 (2010).
37. S. Liehr et al., "Polymer optical fiber sensors for distributed strain measurement and application in structural health monitoring," *IEEE Sens. J.* **9**(11), 1330–1338 (2009).
38. L. Yan et al., "Investigation of an image processing method of step-index multimode fiber specklegram and its application on lateral displacement sensing," *Opt. Fiber Technol.* **46**, 48–53 (2018).
39. P. J. Kajenski, P. L. Fuhr, and D. R. Huston, "Mode coupling and phase modulation in vibrating waveguides," *J. Lightwave Technol.* **10**(9), 1297–1301 (1992).
40. S. Farahi et al., "Dynamic bending compensation while focusing through a multimode fiber," *Opt. Express* **21**(19), 22504–22514 (2013).
41. K. H. Kim, H-S. Lee, and B. Lee, "Enhancement of the wavelength selectivity of a volume hologram by the use of multimode optical fiber referencing," *Opt. Lett.* **23**(15), 1224–1225 (1998).
42. B. Redding and H. Cao, "Using a multimode fiber as a high-resolution low-loss spectrometer," *Opt. Lett.* **37**(16), 3384–3386 (2012).
43. J. Zubia and J. Arrue, "Plastic optical fibers: an introduction to their technological processes and applications," *Opt. Fiber Technol.* **7**(2), 101–140 (2001).
44. A. Kersey et al., "Fiber grating sensors," *J. Lightwave Technol.* **15**(8), 1442–1463 (1997).

Eric Fujiwara is a professor at the University of Campinas, Brazil. He received his BS degree in control and automation engineering from the University of Campinas in 2008, and the MS and PhD degrees in mechanical engineering from the University of Campinas in 2009 and 2012, respectively. He is the author of more than 50 journal and conference papers. His current research interests include optical fiber sensors, fiber specklegram, and human–robot interaction.

Cristiano M. B. Cordeiro is a professor in the Institute of Physics of the University of Campinas (UNICAMP), Campinas, Brazil, with PhD degree in the same university and postdoc from the University of Bath, England. His main research interest is the investigation and development of new optical fibers and their use in optical devices and sensors. He is also interested in the use of addictive manufacturing technologies for optics and photonic applications.

Biographies of the other authors are not available.

Downloaded From: https://www.spiedigitallibrary.org/journals/Optical-Engineering on 08 Oct 2019
Terms of Use: https://www.spiedigitallibrary.org/terms-of-use